Supplementary Figures

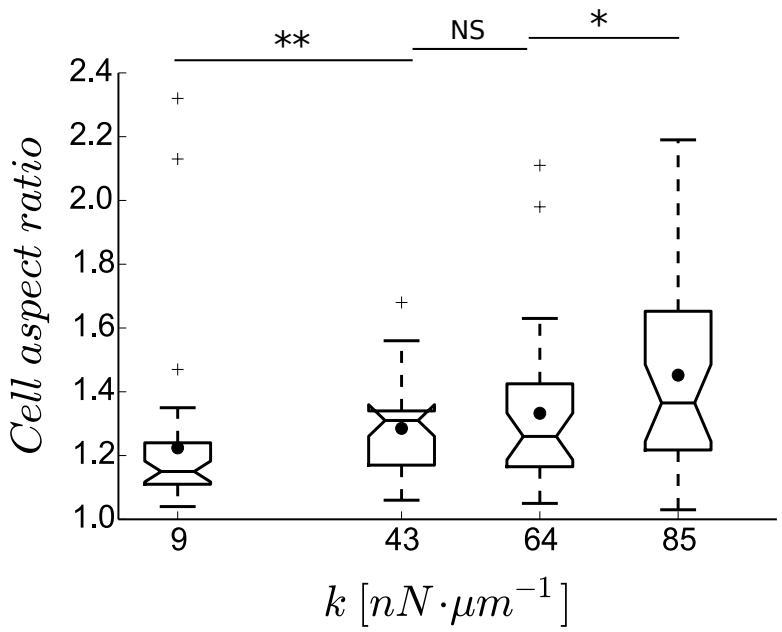

Supplementary Figure 1: **Aspect ratio of cell shape on substrates of different stiffness.** ● represent the mean aspect ratio. Box ends represent the first and third quartiles of the data, and whisker ends represent the last data within 1.5 IQR. Atleast 30 cells were analyzed for each stiffness. P-values were calculated using Mann-Whitney U test. *, $P < 0.05$; **, $P < 0.005$.

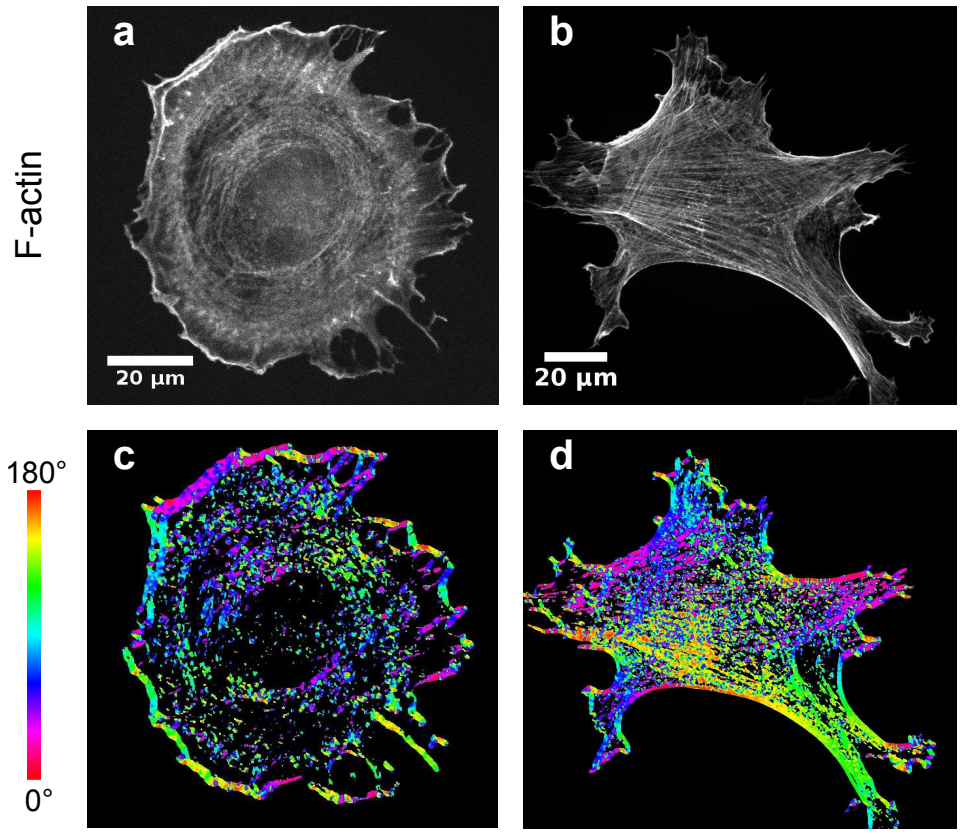

Supplementary Figure 2: **Actin organization on continuous substrates. (a and b)** REF52 cells immunostaind for actin filaments (F-actin) on soft (4 kPa - (a)), and stiff (35 kPa - (b)) polyacrylamide (PAA) gel substrates. **(c and d)** Corresponding orientational plots for actin orientation, where the different colors indicate different orientations of actin filaments as per the given colormap.

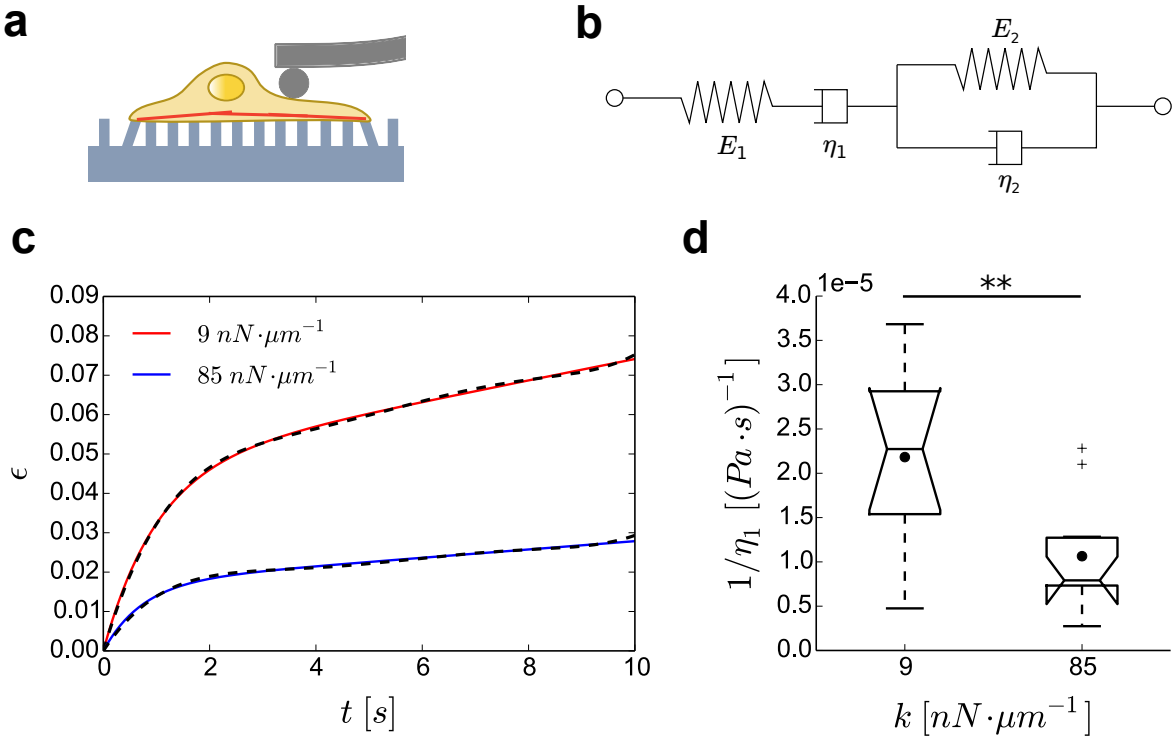

Supplementary Figure 3: **Experimental measurement of cell fluidity. (a)** An AFM tip with a spherical bead was used to probe cell viscoelasticity on micropillar substrates. Live cells were indented with a constant force of 2 nN, held constant for 10 s, and the resulting creep response was measured. **(b)** Schematic of Standard Linear Solid (SLS) model of viscoelasticity used for fitting the obtained creep test data. **(c)** Typical examples of experimental data (dashed black lines), and fitted curves (colored solid lines). **(d)** Fluidity of cells on soft (9 nN·μm^{-1}) and stiff (85 nN·μm^{-1}) substrates. ● represent the mean fluidity. Box ends represent the first and third quartiles of the data, and whisker ends represent the last data within 1.5 IQR. Data was obtained from 10 cells each, with each cell probed at atleast 8 points. $p = 0.007$, from Mann-Whitney U test. E_1 was on the scale of GPa for both soft and stiff substrates, while E_2 increased from 4.02 ± 2.92 kPa on the soft substrate to 6.10 ± 2.92 kPa on the stiff substrate.

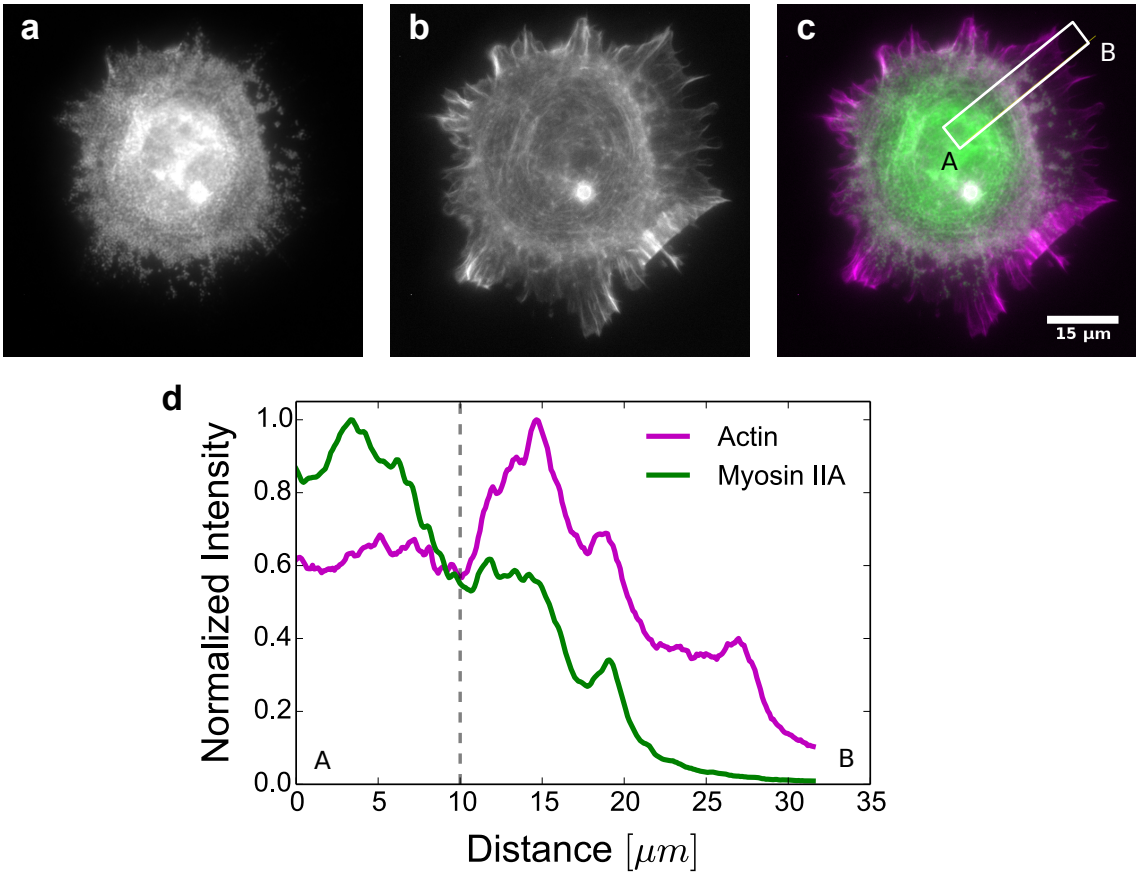

Supplementary Figure 4: **Myosin IIA distribution in cells on soft substrates. (a-c)** REF52 cell immunostained for myosin IIA (*(a)*, in green in *(c)*), and actin filaments (*(b)*, in magenta in *(c)*) on soft (9 nN·μm^{-1}) substrate. **(d)**. Normalized intensity profiles of actin and myosin IIA along the side AB of the white rectangle in *(c)*. The intensities were averaged along the width of the rectangle. The dashed line indicates the nucleus boundary.

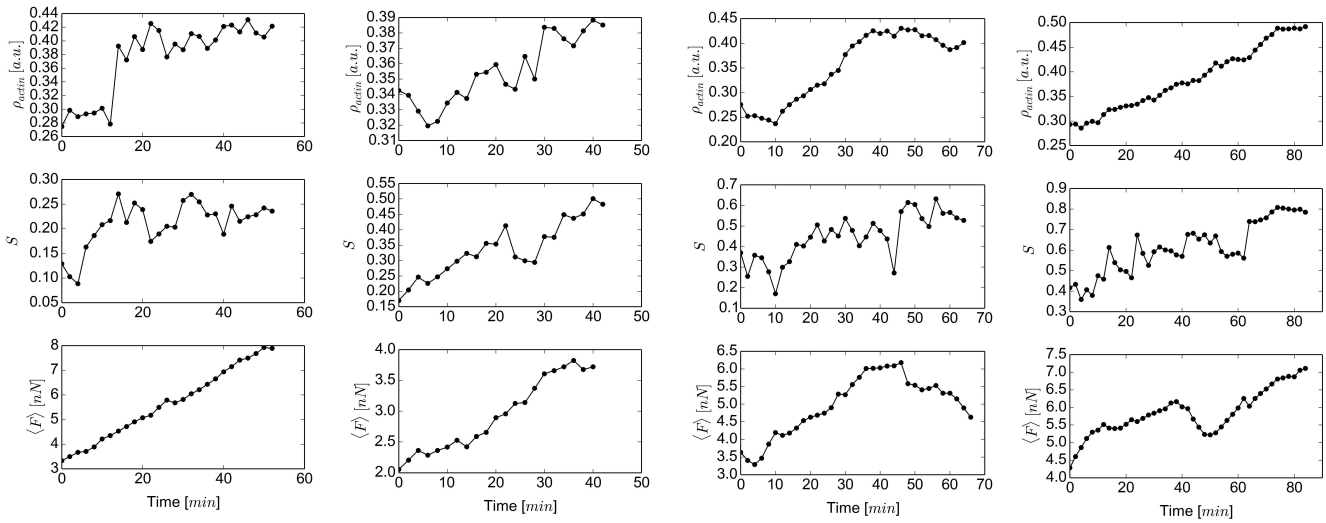

Supplementary Figure 5: **Dynamics of actin stress-fiber micro-domains.** Actin density (mean actin intensity) ρ, actin order parameter S, and mean traction force $\langle F \rangle$ as a function of time. The data was obtained from 5 different actin filament micro-domains, from 5 different cells that were adhered to substrates with stiffness 43 nN$\cdot\mu$m^{-1}.

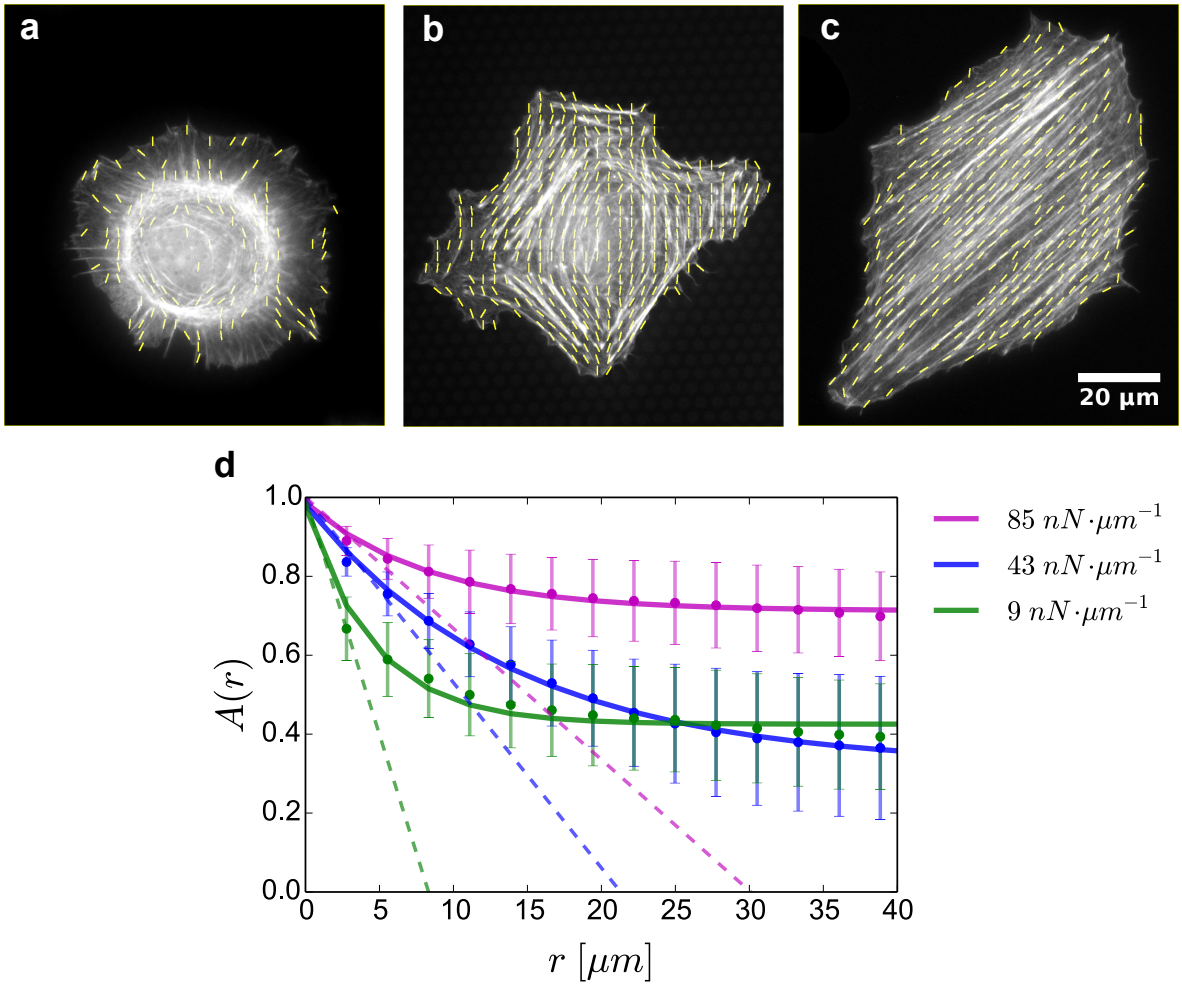

Supplementary Figure 6: **Autocorrelation function of actin filament orientation. (a-c)** REF52 cells immunostained for actin filaments on substrates of stiffnesses 9 nN·μm^{-1} *(a)*, 43 nN·μm^{-1} *(b)*, and 85 nN·μm^{-1} , *(c)* respectively. Yellow lines indicate average local orientation of the filaments. **(d)**. Autocorrelation function of actin orientation, $A(r)$. Solid colored lines represent the exponential expression $ae^{-r/b} + c$, fitted to the data. Dashed lines represent the tangents to the fitted curves at $r = 0$. Their intercept with x-axis gives the auto-correlation length-scales, which are 8, 21, and 30 μm respectively for 9, 43, and 85 nN·μm^{-1} substrates. Data was obtained from 44, 30, and 32 cells for 9, 43, and 85 nN·μm^{-1} substrates respectively. Error bars indicate standard deviations from the mean.

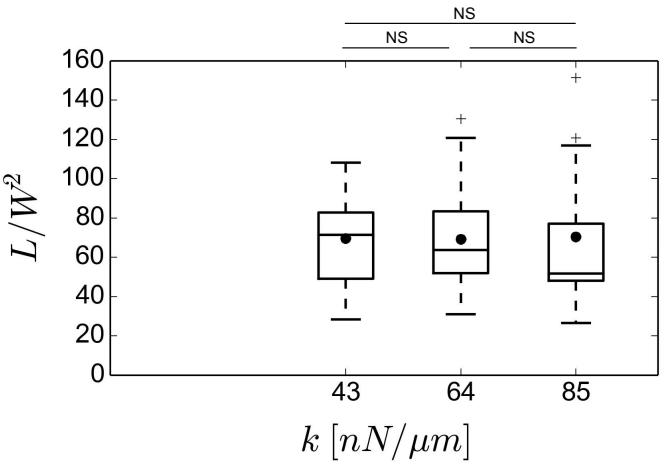

Supplementary Figure 7: **Stress-fiber geometry as a function of substrate stiffness.** L represents the length and W^2 represents the cross-sectional area of stress-fibers. Each data point corresponds to atlest 25 stress-fibers from atleast 5 cells. ● represent the mean values. Box ends represent the first and third quartiles of the data, and whisker ends represent the last data within 1.5 IQR. P-values were calculated using Mann-Whitney U test. NS, $P > 0.01$.

Supplementary Note 1

A. Model hypothesis and notations

The cytoskeleton of a spread cell is modeled as a 2D viscoelastic active gel. The orientational ordering of actin filaments is measured by the nematic order parameter $Q_{ij} = \langle n_i n_j - \delta_{ij}/2 \rangle$, where the average is taken over the local orientation of actin filaments, characterized by a unit vector n_i. Denoting by $\mathbf{e} \equiv \langle \mathbf{n} \rangle$ the local average orientation of actin filaments and $\mathbf{e}_\perp$ its normal, the tensor Q_{ij} is determined in the examples that we describe by the scalar order parameter $S = \langle \cos(2\theta) \rangle$ according to $Q_{\mathbf{ee}} = -Q_{\mathbf{e}_\perp \mathbf{e}_\perp} = S/2$ and $Q_{\mathbf{e}_\perp \mathbf{e}} = Q_{\mathbf{e}\mathbf{e}_\perp} = 0$, where θ is the angle $(\mathbf{e}, \mathbf{n})$.

We assume that the gel is described by a linear Maxwell model of viscoelasticity. The constitutive equation relating the strain rate $v_{ij} = (\partial_i v_j + \partial_j v_i)/2$ to the passive stress tensor $\sigma^{\rm p}_{ij}$ is then written $2\eta v_{ij} = (1 + \tau \frac{D}{Dt}) \sigma^{\rm p}_{ij}$, where η is the shear viscosity and D/Dt denotes the convective derivative. Here τ is a relaxation time, characterized by the typical lifetime of actin structures (bundles or stress fibers) in the cytoskeleton. At time scales $\ll \tau$ actin structures are conserved and the cytoskeleton behaves as a linear elastomer; at time scales $\gg \tau$ the cytoskeleton behaves as a Newtonian fluid. We first argue phenomenologically that τ crucially depends on substrate stiffness. At low stiffness, we observe, in agreement with previous experiments[1], that focal adhesions are small compared to stiff substrates (Fig. 2k). As a consequence, the effective friction between the cytoskeleton and the substrate is very low. Actin is then almost freely convected over the substrate (in response to active constraints due to polymerization and contractility), and the life time of actin structures is bounded by L/v_p (of the order of minutes), where L is a typical cell size and v_p a typical polymerization speed. At the time scale of observations (hours) the cytoskeleton can therefore be considered as viscous, and indeed observations show a sustained flow. On the other hand, at higher substrate stiffnesses, focal adhesion can form and significantly increase friction. In practice actin structures such as stress fibers do not slip over the substrate any more, and their life time is comparable to the observation time. In this regime the cytoskeleton will be described as a linear elastomer.

B. Low stiffness - viscous regime

The viscous regime of nematic active gels has been analyzed quite in depth in the literature. The aim of this section is to show that this framework makes it possible to reproduce the observed actin flows, and that flow alignement effects are sufficient to explain the observed orthoradial actin patterns. Following the active gel theory[2], the active stress can be written $\sigma^{\rm a}_{ij} = \zeta \delta_{ij} + \zeta' Q_{ij}$, so that the total stress finally reads

$$\sigma_{ij} = 2\eta v_{ij} + \zeta \delta_{ij} + \zeta' Q_{ij}. \tag{1}$$

Following observations, we will consider that in this regime the cell remains axisymmetric, and make use of polar coordinates r, θ. Force balance can then be written as

$$\partial_r \sigma_{rr} + \frac{1}{r}(\sigma_{rr} - \sigma_{\theta\theta}) - \partial_r \Pi = \xi v_r \tag{2}$$

where ξ is a friction coefficient and Π is the pressure in the gel. Following[2], the dynamics of Q are coupled to the strain rate tensor. Here we neglect Franck elastic effects, i.e. gradient terms in Q, and assume that the relaxation of Q is fast compared to the time scale of the flow. The nematic order parameter is then slaved to the flow according to

$$S = \alpha(\partial_r - 1/r) v_r \tag{3}$$

where α is a positive coupling constant. Under this assumption that $\alpha > 0$, the gel is in the isotropic phase in absence of flow. Combining the above equations then yields

$$a^2 \left(\partial_r^2 + \frac{\partial_r}{r} - \frac{1}{r^2} \right) v_r - v_r = \frac{1}{\xi} \partial_r \Pi \tag{4}$$

where $a^2 = (2\eta + \zeta' \alpha/2)/\xi$. This equation is solved with $v(r = R) = -v_p$ and $v(r = r_n) = 0$. For the sake of simplicity we assume that the dynamics is mainly driven by boundary conditions and neglect the pressure contribution. The velocity profile then reads:

$$v(r) = A I_1(x/a) + B K_1(x/a) \tag{5}$$

where I, K are Bessel functions and A, B are constants that can be determined explicitly by boundary conditions. A simplified form can be derived for $r \sim R$:

$$v(r) \simeq -v_p e^{\frac{r-R}{a}} \tag{6}$$

which is conveniently used to fit the data. The fit, in good agreement with data, yields an estimate of the length scale a of the order of the cell size. In this regime the order parameter is given by:

$$S(r) \simeq -\frac{\alpha v_p}{a} e^{\frac{r-R}{a}} \tag{7}$$

Since $\alpha > 0$ [2], this indeed predicts an orthoradial organization of actin, as observed experimentally. However, this analysis does not reproduce the behavior of the order parameter close to the cell periphery, where alignement is enforced by polymerization such that $S > 0$. This can be taken into account in the model. Following[2], Eq. (3) should in fact be written:

$$\partial_t S + v_r\, \partial_r S = -\beta_1\, S + \beta_2 \left(\partial_r v_r - \frac{v_r}{r}\right), \tag{8}$$

where the left hand side is the material derivative (note: no co-rotational terms for axisymmetric, centripetal flow), β_1 is an inverse relaxation time, and $\beta_2 > 0$ is the flow ordering parameter. Note that one has $\alpha \equiv \beta_2/\beta_1$. In steady-state, $\partial_t S = 0$.

We assume that in the absence of active effects (polymerization and retrograde flow-driven ordering), the cytoskeleton would be in an isotropic phase (β_1 large and positive and thus $S = 0$). Note that we are neglecting Frank elastic terms $\nabla^2 S$ in the dynamical equation for S, on the basis that the corresponding elastic stiffnesses vary as S^2 and thus are small under the above stated assumption[3].

To calculate $S(r)$ from the flow profile $v_r(r)$, we use the following approximation scheme that takes into account the effect of polymerization at the cell boundary, $r = R$, and of flow ordering:

1. *Effects of boundary polymerization alone.* Actin polymerization at the leading edge, $r = R$, imposes radial order, i.e., $S(R) > 0$. Assuming β_1 is large, S takes large values only near $r = R$ where $v_r \simeq -v_p$. Therefore, the cytoskeletal order resulting from boundary polymerization is obtained by solving $-v_p\, \partial_r S \simeq -\beta_1\, S$, yielding

$$S_{\rm poly} = S(R)\, e^{\frac{\beta_1}{v_p}(r-R)} \tag{9}$$

2. *Effects of flow ordering alone.* Neglecting boundary effects, under the assumption that β_1 is large, we can assume S is slaved to the velocity field. (We are neglecting the convective term in Eq. (8) since it is $\sim v_p^2/\beta_1$, and thus small.) Therefore, the cytoskeletal order due to flow ordering is

$$S_{\rm flow} \simeq \alpha \left(\partial_r v_r - \frac{v_r}{r}\right), \tag{10}$$

   where $\alpha = \beta_2/\beta_1$ as in previous analysis.

3. *Combining boundary and flow ordering effects.* Since it is assumed that $S_{\rm poly}$ decays quickly away from $r = R$, we can combine the effects of polymerization and flow ordering to obtain an approximate, analytical expression for S:

$$S(r) \simeq S_{\rm flow}(r) + (S(R_1) - S_{\rm flow}(R_1))\; e^{\frac{\beta_1}{v_p}(r-R_1)}, \tag{11}$$

   where, R_1 accounts for the condition of normal anchoring of filaments at the cell periphery, and $S_{\rm flow}$ is calculated from Eq. (10) using the calculated profile for v_r:

$$v_r(r) = -\frac{v_p}{K_1(\lambda R) - \frac{I_1(\lambda R)\, K_1(\lambda r_N)}{I_1(\lambda r_N)}} \left[K_1(\lambda r) - \frac{K_1(\lambda r_N)}{I_1(\lambda r_N)}\, I_1(\lambda r)\right]. \tag{12}$$

   Here, K_1 and I_1 are modified Bessel functions of the first kind, r_N is the nuclear radius, and $\lambda = \left(\frac{\xi}{2\eta + \zeta' \alpha/2}\right)^{1/2} \equiv 1/a$ with above notations is the inverse of the friction length scale.

Note that simplified expressions can a priori be used for fitting, see Eq.(6). This yields:

$$S(r) \simeq -\frac{\alpha v_p}{a} e^{\frac{R(r-1)}{a}} + \left(S(R_1) + \frac{\alpha v_p}{a} e^{\frac{R_1-R}{a}}\right) e^{\frac{\Gamma\chi R}{v_p}\left(r-\frac{R_1}{R}\right)} \tag{13}$$

Since $\alpha > 0$ [2], this indeed predicts an orthoradial organization of actin. In this equation the fit parameters are $\Gamma\chi R/v_p$, which is dimensionless; $\alpha v_p/a$, which is dimensionless. Last, the friction length a should be fitted consistently with the velocity profile $v(r)$. Again, for the velocity profile one could take the exact form (12) or more simply (6).

C. High stiffness - elastic regime

In the elastic regime, we introduce the strain tensor $\epsilon_{ij} = (\partial_i u_j + \partial_j u_i)/2$, where $\mathbf{u}$ is the displacement field of the gel. Since we are now interested in the emergence of polarity, we will consider only biaxial deformation and therefore write $\epsilon_{xy} = \epsilon_{yx} = 0$, so that the strain is determined only by its diagonal components. In this section we aim at analyzing the emergence of order at the cell scale. Following[4], we therefore average the tensor order parameter Q (as well as ϵ) spatially over the cell (notations are unchanged for the sake of simplicity). Following[5], we then write down a generic Landau functional that couples ϵ and Q :

$$\mathcal{F}(\epsilon, Q) = \frac{\gamma}{2}(\rho_c - \rho(\epsilon))S^2 + \frac{\omega}{4}S^4 + \mu \mathrm{Tr}(\epsilon \cdot Q) + \mathcal{F}_e(\epsilon) \tag{14}$$

Here ρ is linear in $\mathrm{Tr}(\epsilon)$ and will be interpreted as an effective gel density : $\rho(\epsilon) = \rho_0 + \chi \mathrm{Tr}(\epsilon)$. Here ρ_c, χ are phenomenological coupling constants, which we will argue are positive below. We stress that terms in gradients of Q, as well as boundary terms do not appear in the present mean field discussion in which Q is averaged over the cell; in particular topological defects and domain walls, which seem to be observed, are only effectively taken into account in our approach. $\mathcal{F}_e(\epsilon)$ is the classical quadratic elastic energy. The passive elastic stress in the gel is then classically obtained by differentiating $\mathcal{F}_e$; its contribution is expected to be much smaller than the active stress and will be neglected in what follows. Following earlier works, we write the active stress as

$$\sigma^a_{ij} = \zeta_0 \rho \delta_{ij} + \zeta'_0 \rho Q_{ij}. \tag{15}$$

For the sake of simplicity we assume that the cell interacts with the substrate only through the focal contacts, which are assumed to be located at the cell periphery. Assuming that the reference (undeformed) state has an extension L in both x and y directions, force balance yields $\sigma^a_{ii} + k'(L/A)\epsilon_{ii} = 0$, where A is stress-fiber cross-section area, and k' is substrate stiffness. Here we made use of the fact that the deformations of each of the pillars are independent, and identified the deformation of the gel and of the substrate at the boundary. We found that L/A is constant with substrate stiffness (Supplementary Fig. 7), and hence:

$$\sigma^a_{ii} + k\epsilon_{ii} = 0, \tag{16}$$

where k is proportional to substrate stiffness. This yields:

$$\rho = \frac{\rho_0}{1 + 2\chi\zeta/k}. \tag{17}$$

The dependence on k can be verified experimentally (Supplementary Fig. 5), which confirms that ρ can indeed be interpreted as the gel density. Next we assume that, as in equilibrium, S is obtained by minimizing F

$$\gamma(\rho_c - \rho)S + \omega S^3 + \mu(\epsilon_{xx} - \epsilon_{yy})/2 = 0 \tag{18}$$

This can be rewritten as

$$S\left[\gamma(\rho_c - \rho) - \frac{\mu\zeta'\rho}{2k} + \omega S^2\right] = 0. \tag{19}$$

This shows that the gel undergoes an isotropic/nematic transition similar to lyotropic liquid crystals. For

$$\rho < \rho^* = \frac{\gamma\rho_c}{\gamma + \frac{\mu\zeta'}{2k}} \tag{20}$$

one has $S = 0$ and the system is isotropic. In turn, when $\rho > \rho^*$, the radial symmetry is spontaneously broken and

$$S = \left[\frac{\frac{\mu\zeta'\rho}{2k} - \gamma(\rho_c - \rho)}{\omega} \right]^{1/2} \tag{21}$$

From the dependence of ρ on the substrate stiffness k, we find equivalently that this transition can be controlled by substrate stiffness. Introducing

$$k^* = \frac{\rho_c}{\rho_0 - \rho_c} \left(2\chi\zeta - \frac{\mu\rho_0\zeta'}{2\gamma} \right) \tag{22}$$

we find that the gel is isotropic at low stiffness ($k < k^*$), and nematic at high stiffness ($k > k^*$). This provides a simple stiffness dependent polarisation mechanism, which is in qualitative agreement with observations. As in classical second order phase transitions, this analysis predicts that close to the transition, one has

$$S \propto \sqrt{k - k^*} \tag{23}$$

which agrees well with observations (Fig. 4e). Also, the order parameter for force vectors, $S_\sigma \propto S$ (Fig. 4f). The model also predicts that the average force exerted on pillars, $\langle F \rangle \propto \mathrm{Tr}(\sigma^a) \propto \rho$. Thus,

$$\langle F \rangle \propto \frac{\rho_0}{1 + 2\chi\zeta/k} \tag{24}$$

which agrees well with observations (Fig. 4g), and predicts that $\langle F \rangle$ will saturate to ≈ 9 nN at very high substrate stiffness. Also, the mean elastic energy stored in the substrate,

$$E = \frac{1}{2}(\epsilon_x^2 + \epsilon_y^2) \tag{25}$$

which can be solved using Eqs. (15,16,17) to obtain:

$$E = \frac{c_1/k(1 + c_2/k)}{(1 + 2\chi\zeta/k)^3} \tag{26}$$

where, $c_1 = \frac{\omega\rho_0^2}{\omega\zeta^2 + \gamma(\rho_0 - \rho_c)}$, and $c_2 = \frac{2\gamma\zeta(\omega\zeta^2 - \gamma\rho_c) + \rho_0\mu\zeta'^3}{\omega\zeta^2 + \gamma(\rho_0 - \rho_c)}$.

Several comments are in order. (i) Eq.(14) is a systematic expansion. In particular the coefficient of S^2 is for symmetry reasons linear in $\mathrm{Tr}(\epsilon)$, but the sign of the phenomenological coupling is not known a priori. Our analysis shows the isotropic/nematic transition, compatible with observations, is realized for $\chi > 0$ and $\rho_0 > \rho_c$. While $\chi > 0$ would contradict equilibrium thermodynamics, it is in fact at the core of the active mechanosensing mechanism that we describe. (ii) For similar reasons the sign of μ is not known a priori. This coupling merely results in a shift of the critical point and can be neglected in a first approximation.

Supplementary References

[1] Yeung, T. *et al.* Effects of substrate stiffness on cell morphology, cytoskeletal structure, and adhesion. *Cell Motil. Cytoskeleton* **60**, 24–34 (2005).

[2] Salbreux, G., Prost, J. & Joanny, J. F. Hydrodynamics of cellular cortical flows and the formation of contractile rings. *Phys. Rev. Lett.* **103**, 058102 (2009).

[3] Berreman, D. W. & Meiboom, S. Tensor representation of oseen-frank strain energy in uniaxial cholesterics. *Phys. Rev. A* **30**, 1955–1959 (1984). URL `http://link.aps.org/doi/10.1103/PhysRevA.30.1955`.

[4] Zemel, A., Rehfeldt, F., Brown, A. E., Discher, D. E. & Safran, S. A. Optimal matrix rigidity for stress fiber polarization in stem cells. *Nat. Phys.* **6**, 468–473 (2010).

[5] Lubensky, T. C., Mukhopadhyay, R., Radzihovsky, L. & Xing, X. Symmetries and elasticity of nematic gels. *Phys. Rev. E Stat. Nonlin. Soft Matter Phys.* **66**, 011702 (2002).

[6] Tse, J. R. & Engler, A. J. Preparation of hydrogel substrates with tunable mechanical properties. *Current protocols in cell biology* 10–16 (2010).